NIAR Report 93-18

Supersonic Flow Visualization Of a Nacelle in Close Proximity To a Simulated Wing

Kasim Biber
David R. Ellis

August 1993

NIAR
National Institute for Aviation Research

The Wichita State University
Wichita, Kansas 67260-0093

FINAL TECHNICAL REPORT

NIAR Report 93-18

SUPERSONIC FLOW VISUALIZATION OF A NACELLE IN CLOSE PROXIMITY TO A SIMULATED WING

by

Kasim Biber and David R. Ellis

National Institute for Aviation Research
Wichita State University
Wichita, KS 67260

Contract # : A24888D(MXR)
Technical Monitor: Joel Mendoza
NASA Ames Research Center
Moffett Field, California

July 1993

Supersonic Flow Visualization of a Nacelle in Close Proximity to a Simulated Wing

by

Kasim Biber and David R. Ellis
National Institute for Aviation Research
Wichita State University
Wichita, Kansas 67260

Abstract

A flow visualization study was made in the 9×9-inch supersonic wind tunnel at Wichita State University to examine shock and boundary layer flow interaction for a nacelle in close proximity to the lower surface of a simulated wing. The test matrix included variations of angle of attack from $-2°$ to $+4°$, nacelle-wing gap from 0.5- to 3-nacelle inlet diameter (0.12-inch) and Reynolds number based on nacelle length (1.164-inch) from 1.16×10^6 to 1.45×10^6 at a nominal Mach number of 2. Schlieren pictures of wing and nacelle flowfield were recorded by a video camera during each tunnel run. Results show that the nacelle inlet shock wave remains attached to the inlet lip and its impingement does not significantly affect the wing boundary layer. At the nacelle trailing edge location, the wing boundary layer thickness is approximately one-nacelle inlet diameter at $\alpha = 0°$ and it decreases with increase of angle of attack.

Table of Contents

List of Tables

List of Figures

Nomenclature

D	nacelle inlet diameter : 0.12-inch
M	test Mach number : 1.94
P_T	settling chamber pressure : 42 and 52 psia [lb/in^2]
Re_L	Reynolds number based on nacelle length : 1.16×10^6 and 1.45×10^6
Re/ft	Reynolds number based on a foot : 12×10^6 and 15×10^6
x	horizontal downstream distance from the wing leading edge
Y	vertical spacing between wing and nacelle : 0.06, 0.12, 0.24, and 0.36-inch
Y/D	wing-nacelle gap : 0.5, 1, 2, and 3
α	angle of attack : $-2°$, $0°$, $+2°$, and $+4°$
δ	boundary layer thickness, [inch]

1. INTRODUCTION

Nacelle/airframe integration is of major importance for aerodynamically efficient supersonic transport aircraft design and development.[1,2] For such aircraft, the nacelles are commonly positioned beneath the wing to produce relatively low wave drag. Figure 1 shows a typical nacelle/wing arrangement used for computational studies[3,4] of interference effects. In its proper location, the nacelle should normally have an attached normal shock at its inlet lip and capture the oncoming air mass without any spillage (Figure 2a). If the mass flow through the nacelle was reduced by using, for instance a flow restrictor as in Fig. 2b, then the normal shock wave would move upstream progressively and become detached from the inlet lip. In this case, the subsonic flow behind the detached shock would involve with spillage drag, which would degrade engine thrust.[5] Flow through such isolated nacelles was visualized in an early study made at the Wichita State University.[6]

When a nacelle is integrated with an aircraft wing, its flowfield is affected by the wing boundary layer, depending on the nacelle proximity to the wing surface. If the nacelle inlet is placed completely outside the boundary layer (as in Fig. 3a), then there will be an increase of wave drag. If the wing boundary layer flows through the nacelle (as in Fig 3b), then loss in total pressure and distortion in the velocity distribution will result, causing a reduction in the engine flow cycle[7]. Therefore, the boundary layer is removed by means of bleed and diverter before it enters to the nacelle.[5,7] However, such a boundary layer control requires a detailed knowledge of both isolated and integrated wing-nacelle flowfields at various Reynolds numbers, angles of attack and wing-nacelle gaps.

This report presents the results of a flow visualization study featuring wind tunnel tests of a simulated flow-through nacelle with a sharp-lip pitot intake under a flat planform wing with swept back subsonic leading edge. The study brings some insight into the shock-boundary layer interaction between the nacelle and the wing. The test matrix included variations of angle of attack from $-2°$ to $+4°$, wing-nacelle gap from half- to three-nacelle inlet diameter and Reynolds number based on the nacelle length from 1.16×10^6 to 1.45×10^6 at a nominal Mach number of 2.

2. EXPERIMENTAL ARRANGEMENT

2.1 Wind Tunnel

The tests were conducted in the 9 × 9-inch supersonic wind tunnel at Wichita State University (WSU) (see Figure 4). The tunnel is a pressure driven, intermittent and open circuit blowdown design. It has the capability of operating at Mach numbers of 2, 3 and 4 by utilizing fixed contour nozzle blocks. The tunnel is equipped with a closed-loop servo mechanism that keeps the settling chamber pressure constant during the tunnel run. Details of the tunnel and its control mechanism are given in Reference 8.

2.2 Test Model

The test model used was a nacelle in close proximity to a simulated wing. The nacelle was designed in the form of a sharp-lip pitot intake with 0.12-inch diameter, through-flow duct with 1.164-inch length and a truncated-conical exterior with 2.5° semi-vertex angle, as shown in Figure 5. It was mounted to the tunnel C-strut assembly through its pylon. At its zero angle of attack setting, the nacelle was aligned with the test section centerline. The same nacelle had been used in the previous isolated nacelle tests[6] (the so-called Model 3) at WSU.

The wing was designed to simulate a delta wing with a swept subsonic leading edge in the form of 0.25-inch thick, 9-inch long and 3-inch wide flat plate planform with a 60° sweepback angle, as shown in Figure 6. When installed in the test section, the wing was above the nacelle and parallel to the nacelle centerline, and supported separately from the nacelle so that there was no nacelle-wing strut to cause additional interference (see Figure 7). The wing assembly was supported by both the C-strut and a vertical strut placed further downstream near the tunnel diffuser to provide additional stability (see Figure 8). The wing positions with respect to the nacelle was indexed on a block so that the gap distance between the nacelle trailing edge and the wing could be set to 0.5, 1, 2 and 3 nacelle inlet diameters (0.06, 0.12, 0.24 and 0.36 inches respectively). The wing-nacelle gap was set when $\alpha = 0°$. For each wing-nacelle gap, the model angle of attack changes were made in the order of $-2°$, $0°$, $+2°$ and $+4°$.

2.3 Test Conditions

Test conditions were characterized by the settling chamber pressure for the flow produced by the Mach 2 nozzle blocks. Considering the losses at the downstream of the nozzle throat (see Ref. 9), the actual test Mach number was 1.94, as determined from shock wave angle over the simulated wing, and the ratio of test section pitot pressure to settling chamber pressure.

Reynolds number was calculated from the settling chamber pressure and temperature for the prescribed Mach number. The viscosity was determined from Sutherland's formula as given in Reference 10. Tests were made for settling chamber pressures of 42 and and 52 psia, corresponding to Reynolds number based on nacelle length (1.164-inch) of 1.16×10^6 and 1.45×10^6 respectively. Table 1 shows complete test cases. The settling chamber pressure and therefore Reynolds number range was limited by the nacelle/pylon strength.

The flow unsteadiness in the settling chamber was observed qualitatively by time history of stagnation pressures for about 10 seconds of tunnel runs.[8] There were fluctuations on the pressure signals, but these were below $\pm 5\%$ for the present test values. These fluctuations apparently caused some vibration on the nacelle model during runs. Because of its rather thin shape to prevent flow interference with the nacelle, the nacelle/pylon failed during the last tunnel run (Run 72) shown in Table 1.

2.4 Flow Visualization Technique

The schlieren method in a "Z" arrangement was used to visualize shock and boundary layer flow patterns. The method provides a picture of variations of density gradients in the two-dimensional plane of flow field[11] by using the set up shown in Figure 9. Obtaining satisfactory picture quality required a careful adjustment of apparatus used for the schlieren set up. A knife edge was placed horizontally near the second mirror focal point to highlight boundary layer effects and shock-boundary layer flow patterns. The focal plane was rectangular with a length-to-width ratio of 4. The model image was viewed on a white screen, upside down due to lack of a third mirror to reflect the image back to its original orientation. The schlieren pictures on the viewing screen were recorded by using an 8 mm video camera. Test

cases were identified orally on the video during the tunnel runs, and later they were transcribed onto white title cards during editing. Table 1 shows a list of test cases shown on the 8 mm video tape.

3. RESULTS AND DISCUSSION

Results of this study are presented on still pictures taken from the video tape. They are not as clear as the video. The hand drawn sketches should illustrate some details for wing-nacelle test cases. As stated previously, images are upside down on the video tape because of the mirror arrangement. Here results are given for only the higher Reynolds number case. In fact, there is not a qualitative difference of shock-boundary layer flow characteristics at Reynolds number of either 1.16×10^6 or 1.45×10^6. However, the higher Reynolds number case provided sharper images of the model flowfield. Tunnel runs were made for tests of wing alone, nacelle alone and then wing and nacelle together.

3.1 Wing Alone Tests

The simulated wing was first tested to check if there was any blockage or design problem in the tunnel test section and also to visualize the shock and boundary layer flow patterns of the wing lower surface when there was no nacelle present. The visualized boundary layer thickness was compared with the one calculated at $\alpha = 0°$ by using the flat plate approximations[12] given for incompressible flow. The calculation was made for the higher Reynolds number case, which corresponds to a local Reynolds number of 9×10^6 at 7.164 inches downstream from the wing leading edge. The comparison is given below:

Flat Plate at $\alpha = 0°$	δ at x = 7.164-inch
Laminar-Incompressible	0.012-inch
Turbulent-Incompressible	0.1-inch
Experiment at M = 1.94	0.12-inch

It was concluded that the wing lower surface boundary layer was tripped to turbulent in character from the wing leading edge. Also, comparison with the wing and nacelle tests showed that the nacelle presence did not change the wing flowfield significantly. Therefore, the wing alone tests were not presented on the final copy of the video tape.

3.2 Nacelle Alone Tests

The nacelle alone flowfield was visualized for comparison when the nacelle was positioned under the simulated wing. As shown in Figs. 10-13, a conical oblique shock wave forms at the nacelle inlet lip and its orientation with the freestream flow changes with the angle of attack. It remains attached to the inlet lip and is symmetric only when $\alpha = 0°$. In fact, at $\alpha = +4°$, an expansion wave could be expected at the leeward side of the nacelle (remember the semi-vertex angle is 2.5°), but this is not noticable on the pictures. The schlieren method, which is sensitive to variations of density gradients and not change of directions, is evidently not sensitive enough to detect this expansion.

There is also a normal shock at the nacelle inlet, although it is not seen on the pictures. The normal shock may not be exactly at the nacelle leading edge but just a little bit downstream of the nacelle intake, interacting with the internal boundary layer of the ducted nacelle. It naturally remains normal to the freestream flow at all angles of attack. Therefore, the normal shock orientation with the nacelle leading edge is altered with the angle of attack changes. That is, at $\alpha = -2°$ the normal shock is more upstream on the inlet lower side than that on the upper side, and at $\alpha = +2°$ the reverse of this is true. In fact, at a sufficiently high angle of attack (say 10°), the normal shock might be detached from only the upper side of the inlet. However, as can seen from the figures, this detachment did not occur during the present tests, probably because the highest angle of attack was only +4°. The leading edge shock wave has some curvature near the inlet lip, as shown in the figures. This is also believed to be due to changes in the normal shock orientation with the nacelle leading edge in addition to the flow turbulence and the model vibration.

The nacelle boundary layer is not visible on the recorded pictures. This means that the nacelle boundary layer is evidently quite thin, and that there is not any indication of nacelle boundary layer separation due to the leading edge shock waves. In fact, the nacelle has a conical exterior with 2.5° semi-vertex cone angle. Therefore, it is subject to three-dimensional exterior flowfield at angles of attack. The flow three-dimensionality has apparently a favorable effect on the nacelle boundary layer behaviour.

The flow through the ducted nacelle expands to the freestream at the nacelle exit. The flow inside the duct is evidently fully turbulent and free of shock waves. This was mainly because the nacelle length-to-inlet diameter ratio (L/D = 9.7) was not large enough for the internal boundary layer to create any choking flow conditions and subsequent supersonic flow in the duct (see Reference 13). In other words, the exit flow is subsonic and has relatively high pressure and hence expands to a lower back pressure region. The schlieren pictures show the free-jet boundary running away from the nacelle centerline. The expansion waves from the nacelle exit on the other hand merge with each other at about nacelle centerline when $\alpha = 0°$ (presumably symmetric flow). However, at angles of attack, there is a distortion of symmetry even though it is not very significant on the pictures.

3.3 Wing and Nacelle Tests

The tests were made with the nacelle positioned 6-inch downstream from the wing leading edge and at several distances below the wing horizontal centerline. The wing clearance from the nacelle (Y) was measured from the wing-side of the nacelle trailing edge and normalized with the nacelle inlet diameter (D). The angle of attack changes were made simultaneously for both the wing and nacelle for a prescribed gap between them. At its test position, the nacelle was in a flowfield with a local Mach number slightly higher than the freestream Mach number at $\alpha = -2°$ due to expansion waves, and lower than the freestream Mach number at $\alpha = +2°$ and $+4°$ due to compression waves from the wing leading edge. Furthermore, there was no change of Mach number when $\alpha = 0°$. Another effect considered was the influence of vorticity generated along the swept back wing leading edge when the model angle of attack was negative ($\alpha = -2°$). It was believed that the vorticity was insignificant and washed away without having much effect on the nacelle flowfield. The shock-boundary layer interaction between the nacelle and the wing was visualized for four different wing-nacelle gap cases and discussed in the subsequent sections.

Results for Y/D = 3 Case: As shown in Figs. 14 and 15, the nacelle is far below the wing and is not influenced by the wing boundary layer. The wing boundary layer gets thinner with increase in angle of attack. There are shock waves from the edges of the wing where the sweep ends. This wave becomes significant only when $\alpha = -2°$ (see Fig. 14), but has no apparent effect on the nacelle flowfield.

By looking carefully at the second picture in Fig. 14, a free arc shape wave can be seen extending across the vertical plane of test section where the nacelle is under the wing. It is not clear what causes this wave. It also occurs in all other test cases when $\alpha = -2°$. In fact, the arc wave gradually disappears as the angle of attack increases to $\alpha = +4°$, as also evidenced in the other test cases discussed later.

The leading edge shock and exhaust free-jet layer at the nacelle wing-side impinge on the wing boundary layer and reflect back towards the nacelle. The shock impingement apparently does not have any effect on the already turbulent wing boundary layer. The reflection patterns are very similar at both $\alpha = -2°$ and $+4°$ except that shock wave angles change with the angle of attack and as do the reflected wave angles. Furthermore, there is a slight distortion of symmetry on the nacelle exhaust flow for non-zero angles of attack, as evidenced from the location where the expansion waves cross each other.

Results for Y/D = 2 Case: As shown in Figs. 16 and 17, the nacelle is clear from the wing boundary layer about one-nacelle inlet diameter. The trends of the shock-boundary layer interaction are similar to the Y/D = 3 test case. However, in this case the nacelle leading edge shock waves are reflected back from the wing surface to the nacelle upper (leeward for $\alpha \geq 0°$) side at further upstream locations.

Results for Y/D = 1 Case: At $\alpha = 0°$, the wing boundary layer is tangent to the nacelle trailing edge (see Figures 18-21). In other words, the wing boundary layer thickness fills the gap between the wing and nacelle. Furthermore, the boundary layer thickness changes slightly with angle of attack.

The leading edge shock impinges on the boundary layer and reflects back to the nacelle in a relatively short downstream distance. This impingement normally goes through the subsonic boundary layer until it reaches the solid surface, and its effect is felt in a region subject to an increase in the pressure. The pressure rise associated with the shock system is apparently not high enough to cause any boundary layer separation as seen from the pictures. However, as explained in Ref. 14, there are compression waves generated by the pressure change in the subsonic layer and these waves coalesce with the reflected wave in and out of the boundary layer. In fact, Ref. 14 also states that the turbulent boundary layer thickness should decrease because of the interaction, but this is not evident from the present

results. The pictures show no sign of change in the boundary layer thickness due to the leading edge shock impingement. There is also a possibility of merging of the nacelle and wing boundary layers, but again this is not observed on the schlieren pictures. The nacelle exhaust flow is similar to the preceding two test cases, except that its wing-side is absorbed by the wing boundary layer.

Results for Y/D = 0.5 Case: One important aspect of the present study was to bring the nacelle as close to the wing as possible and observe the interference effects. For this reason, the nacelle was positioned so that its inlet could be partially inside the wing boundary layer. As shown in the pictures (Figs. 22-25), the nacelle leading edge shock wave at the wing-side is completely absent and there is an attached shock wave from the nacelle lower (windward for $\alpha \geq 0°$) side. The wing boundary layer appears to have no effect on the inlet normal shock.

For the thickest boundary layer (at $\alpha = -2°$), a small fraction of the wing boundary layer is entering to the nacelle. As it travels inside the nacelle duct, it evidently thickens the internal boundary layer and partially distorts the internal velocity distribution. How much thickness the wing boundary layer adds to the duct is not seen on the pictures, but its effect on the flowfield becomes more pronounced at the nacelle exit. The wing boundary layer just after the nacelle shows an increased thickness, and it prevents the formation of one of the branches of the exit expansion waves. The increase of thickness is also as a result of the additional turbulence produced by the nacelle entry to the wing boundary layer. As the angle of attack is increased from $-2°$ to $+4°$, there is a decrease in the wing boundary layer entering to the duct and hence in the boundary layer thickness just downstream from the nacelle. Furthermore, the nacelle exhaust flow appears to show a lessened effect of the wing boundary layer impingement.

For this test case, the nacelle exit flow discharges into the wing boundary layer flow. Since the boundary layer has lower velocity than both the freestream and the nacelle exit flow, an over-expansion wave pattern occurs for the region where the nacelle exit is inside the wing boundary layer. The occurence of both under- and over-expansion flow for the same nacelle exit flow creates a rather complex phenomenon and not clearly defined in the pictures. The merits of designing nacelles which do not ingest boundary layer flow are evident from these pictures.

3.4 Future Work

The present study was made over relatively small range of angle of attack and Reynolds number, mainly due to the supersonic wind tunnel limitations. Therefore, there was not a significant difference in pictures obtained at either Reynolds number of 1.16×10^6 or 1.45×10^6. It is known that boundary layer thickness of wing lower surface increases with decrease of either Reynolds number or angle of attack. If a study were made over a relatively wider range of Reynolds numbers even with the present test angles of attack, there would be considarable information regarding the shock-boundary layer interaction phenomena. In fact, a typical supersonic transport aircraft operates at a cruise Reynolds number based on its nacelle length (say 12.5 foot) in the range of about 3×10^7 at 50,000 foot altitude. This means that the test Reynolds number was about 25 times lower than its flight counterpart.

Tests should be conducted for nacelles with reduced internal flow to produce a detached shock in front. The detached shock wave interaction with the wing boundary layer and subsequent mass flow spillage at the nacelle lip would be interesting phenomena to visualize. This could be done by using the nacelle model with a flow restrictor inside. The shock detachment characteristics could be studied by using flow restrictors with various internal diameters.

4. CONCLUSIONS

A flow visualization study was made in the 9×9-inch supersonic wind tunnel at Wichita State University to examine the shock and boundary layer flow patterns between a nacelle and a simulated wing. Schlieren pictures recorded on a video tape support the following conclusions:

1) The nacelle leading edge shock wave appears to be attached to the inlet lip for all test cases.

2) The boundary layer on the wing lower surface is turbulent and the shock-expansion waves from the nacelle do not have a significant impingement effect on its character. At large wing-nacelle gaps (Y/D = 2 and 3), the shock-expansion waves are reflected from the boundary layer back towards the nacelle wing-side.

3) When the wing-nacelle gap is set to Y/D = 1, the wing boundary layer thickness becomes equal to the wing-nacelle gap at the nacelle trailing edge at zero angle of attack.

4) For the smallest gap (Y/D = 0.5), the nacelle inlet is partially inside the wing boundary layer. At $-2°$ of angle of attack, some boundary layer enters the nacelle and distorts the nacelle exhaust flow symmetry. The amount of wing boundary layer flowing through the nacelle and the associated distortion are lessened with increase in angle of attack.

5. REFERENCES

[1] Rech, J. and Leyman, C.S., "Concorde Aerodynamics and Associated Systems Development", AIAA Professional Study Series, 1980.

[2] Ferri, A., "Airframe/Engine Integration", AGARD Lecture Series No. 53, May 1972.

[3] Mack, R.J., "A Numerical Method for Evaluation and Utilization of Supersonic Nacelle-Wing Interference", NASA TN D-5057, March 1969.

[4] Harris, R.V., "A Numerical Technique for Analysis of Wave Drag at Lifting Conditions", NASA TN D-3586, October 1966.

[5] Seddom, J. and Goldsmith, E.L., Intake Aerodynamics, AIAA Education Series, 1985.

[6] Irani, E. and Ellis, D.R., "Supersonic Wind Tunnel Visualization of Shock Structures on Flow Through Engine Nacelles", Wichita State University, NIAR Report 92-16, August 1992.

[7] Kuchemann, D., The Aerodynamic Design of Aircraft, Pergamon Press, 1978.

[8] Biber, K., "Calibartion and Use of WSU 9 × 9-inch Supersonic Wind Tunnel", Wichita State University, NIAR Report 93-17, January 1993.

[9] Pope, A. and Goin, L.K., High-Speed Wind Tunnel Testing, Krieger, Inc., Malabar, FL, 1965.

[10] NASA Ames Research Staff, "Equations, Tables, and Charts for Compressible Flow", NACA 1135 Report, 1953.

[11] Merzkirch, W., Flow Visualization, Academic Press, 1974.

[12] Schlichting, H., Boundary-Layer Theory, Seventh Edition, McGraw-Hill Co., 1979.

[13] Shapiro, A.H., The Dynamics and Thermodynamics of Compressible Fluid Flow, Volume I and II, The Ronald Press Co., 1954.

[14] Green, J.E., "Interactions Between Shock Waves and Turbulent Boundary Layers", Progress in Aerospace Sciences, edited by D. Kuchemann, Pergamon Press, 1970, pp. 235-340.

Table 1: Test cases presented on the Hi 8 mm video tape*

No	Test	α	Y/D	P_T(psia)	Re_L	Re/ft	M
1	Nacelle Alone	−2°	–	42	1.16×10^6	12×10^6	1.94
2	Nacelle Alone	−2°	–	52	1.45×10^6	15×10^6	1.94
3	Nacelle Alone	0°	–	42	1.16×10^6	12×10^6	1.94
4	Nacelle Alone	0°	–	52	1.45×10^6	15×10^6	1.94
5	Nacelle Alone	+2°	–	42	1.16×10^6	12×10^6	1.94
6	Nacelle Alone	+2°	–	52	1.45×10^6	15×10^6	1.94
7	Nacelle Alone	+4°	–	42	1.16×10^6	12×10^6	1.94
8	Nacelle Alone	+4°	–	52	1.45×10^6	15×10^6	1.94
9	Wing/Nacelle	−2°	0.5	42	1.16×10^6	12×10^6	1.94
10	Wing/Nacelle	−2°	0.5	42	1.16×10^6	12×10^6	1.94
11	Wing/Nacelle	−2°	0.5	52	1.45×10^6	15×10^6	1.94
12	Wing/Nacelle	−2°	0.5	52	1.45×10^6	15×10^6	1.94
13	Wing/Nacelle	0°	0.5	42	1.16×10^6	12×10^6	1.94
14	Wing/Nacelle	0°	0.5	42	1.16×10^6	12×10^6	1.94
15	Wing/Nacelle	0°	0.5	52	1.45×10^6	15×10^6	1.94
16	Wing/Nacelle	0°	0.5	52	1.45×10^6	15×10^6	1.94
17	Wing/Nacelle	+2°	0.5	42	1.16×10^6	12×10^6	1.94
18	Wing/Nacelle	+2°	0.5	42	1.16×10^6	12×10^6	1.94
19	Wing/Nacelle	+2°	0.5	52	1.45×10^6	15×10^6	1.94
20	Wing/Nacelle	+2°	0.5	52	1.45×10^6	15×10^6	1.94
21	Wing/Nacelle	+4°	0.5	42	1.16×10^6	12×10^6	1.94
22	Wing/Nacelle	+4°	0.5	42	1.16×10^6	12×10^6	1.94
23	Wing/Nacelle	+4°	0.5	52	1.45×10^6	15×10^6	1.94
24	Wing/Nacelle	+4°	0.5	52	1.45×10^6	15×10^6	1.94

Note that the wing/nacelle runs were repeated for each test case: the whole wing/nacelle flowfield was filmed on the first run, while only the region close to the nacelle was captured on the second.

Table 1: Continued

No	Test	α	Y/D	P_T(psia)	Re_L	Re/ft	M
25	Wing/Nacelle	$-2°$	1	42	1.16×10^6	12×10^6	1.94
26	Wing/Nacelle	$-2°$	1	42	1.16×10^6	12×10^6	1.94
27	Wing/Nacelle	$-2°$	1	52	1.45×10^6	15×10^6	1.94
28	Wing/Nacelle	$-2°$	1	52	1.45×10^6	15×10^6	1.94
29	Wing/Nacelle	$0°$	1	42	1.16×10^6	12×10^6	1.94
30	Wing/Nacelle	$0°$	1	42	1.16×10^6	12×10^6	1.94
31	Wing/Nacelle	$0°$	1	52	1.45×10^6	15×10^6	1.94
32	Wing/Nacelle	$0°$	1	52	1.45×10^6	15×10^6	1.94
33	Wing/Nacelle	$+2°$	1	42	1.16×10^6	12×10^6	1.94
34	Wing/Nacelle	$+2°$	1	42	1.16×10^6	12×10^6	1.94
35	Wing/Nacelle	$+2°$	1	52	1.45×10^6	15×10^6	1.94
36	Wing/Nacelle	$+2°$	1	52	1.45×10^6	15×10^6	1.94
37	Wing/Nacelle	$+4°$	1	42	1.16×10^6	12×10^6	1.94
38	Wing/Nacelle	$+4°$	1	42	1.16×10^6	12×10^6	1.94
39	Wing/Nacelle	$+4°$	1	52	1.45×10^6	15×10^6	1.94
40	Wing/Nacelle	$+4°$	1	52	1.45×10^6	15×10^6	1.94
41	Wing/Nacelle	$-2°$	2	42	1.16×10^6	12×10^6	1.94
42	Wing/Nacelle	$-2°$	2	42	1.16×10^6	12×10^6	1.94
43	Wing/Nacelle	$-2°$	2	52	1.45×10^6	15×10^6	1.94
44	Wing/Nacelle	$-2°$	2	52	1.45×10^6	15×10^6	1.94
45	Wing/Nacelle	$0°$	2	42	1.16×10^6	12×10^6	1.94
46	Wing/Nacelle	$0°$	2	42	1.16×10^6	12×10^6	1.94
47	Wing/Nacelle	$0°$	2	52	1.45×10^6	15×10^6	1.94
48	Wing/Nacelle	$0°$	2	52	1.45×10^6	15×10^6	1.94
49	Wing/Nacelle	$+2°$	2	42	1.16×10^6	12×10^6	1.94
50	Wing/Nacelle	$+2°$	2	42	1.16×10^6	12×10^6	1.94
51	Wing/Nacelle	$+2°$	2	52	1.45×10^6	15×10^6	1.94
52	Wing/Nacelle	$+2°$	2	52	1.45×10^6	15×10^6	1.94
53	Wing/Nacelle	$+4°$	2	42	1.16×10^6	12×10^6	1.94
54	Wing/Nacelle	$+4°$	2	42	1.16×10^6	12×10^6	1.94
55	Wing/Nacelle	$+4°$	2	52	1.45×10^6	15×10^6	1.94
56	Wing/Nacelle	$+4°$	2	52	1.45×10^6	15×10^6	1.94

Table 1: Concluded

No	Test	α	Y/D	P_T(psia)	Re_L	Re/ft	M
57	Wing/Nacelle	$-2°$	3	42	1.16×10^6	12×10^6	1.94
58	Wing/Nacelle	$-2°$	3	42	1.16×10^6	12×10^6	1.94
59	Wing/Nacelle	$-2°$	3	52	1.45×10^6	15×10^6	1.94
60	Wing/Nacelle	$-2°$	3	52	1.45×10^6	15×10^6	1.94
61	Wing/Nacelle	$0°$	3	42	1.16×10^6	12×10^6	1.94
62	Wing/Nacelle	$0°$	3	42	1.16×10^6	12×10^6	1.94
63	Wing/Nacelle	$0°$	3	52	1.45×10^6	15×10^6	1.94
64	Wing/Nacelle	$0°$	3	52	1.45×10^6	15×10^6	1.94
65	Wing/Nacelle	$+2°$	3	42	1.16×10^6	12×10^6	1.94
66	Wing/Nacelle	$+2°$	3	42	1.16×10^6	12×10^6	1.94
67	Wing/Nacelle	$+2°$	3	52	1.45×10^6	15×10^6	1.94
68	Wing/Nacelle	$+2°$	3	52	1.45×10^6	15×10^6	1.94
69	Wing/Nacelle	$+4°$	3	42	1.16×10^6	12×10^6	1.94
70	Wing/Nacelle	$+4°$	3	42	1.16×10^6	12×10^6	1.94
71	Wing/Nacelle	$+4°$	3	52	1.45×10^6	15×10^6	1.94
72	Wing/Nacelle	$+4°$	3	52	1.45×10^6	15×10^6	1.94

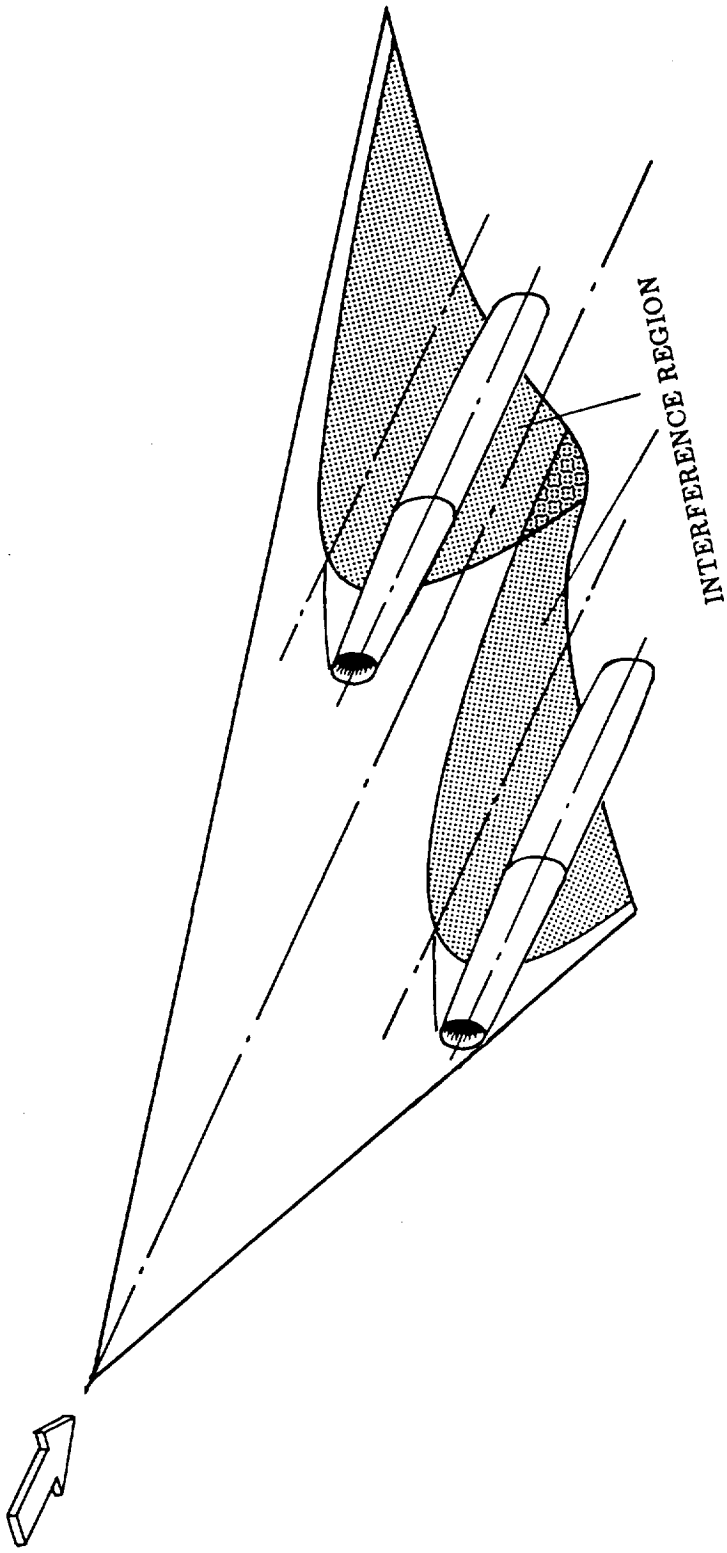

Figure 1 : Typical nacelle-wing arrangement for a supersonic transport aircraft with underwing interference region, Reference 3.

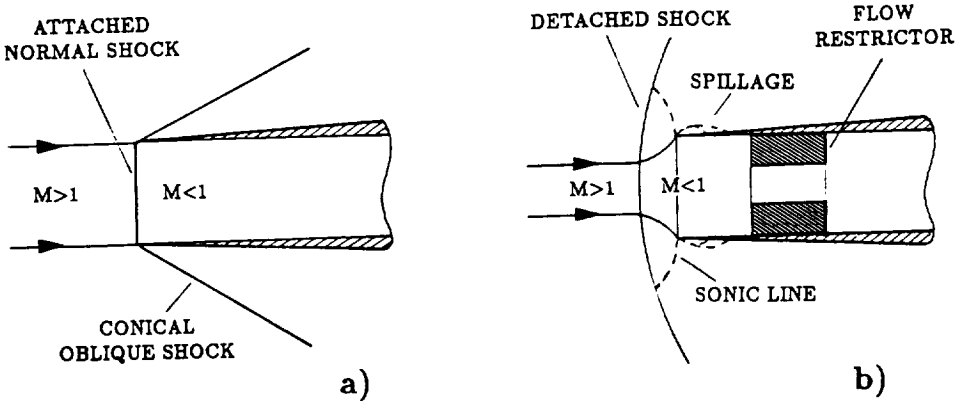

Figure 2 : Attached/detached shock flow position for a sharp-lip pitot nacelle inlet: a) Attached normal shock to the inlet lip, b) Detached shock with flow restrictor inside the nacelle.

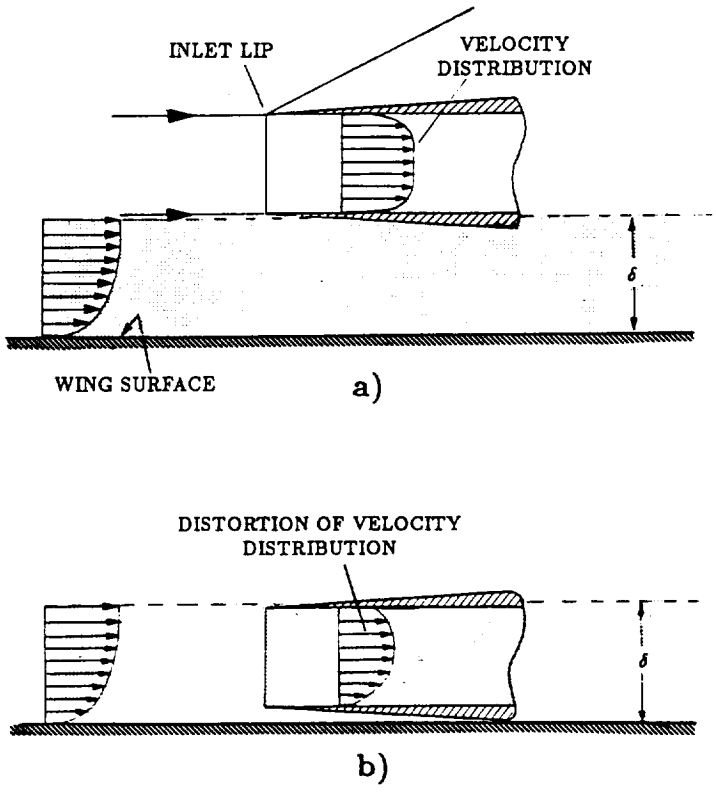

Figure 3 : Nacelle inlet position with respect to the wing boundary layer: a) Non-affected inlet internal flow, b) Distorted inlet internal flow due to boundary layer injection.

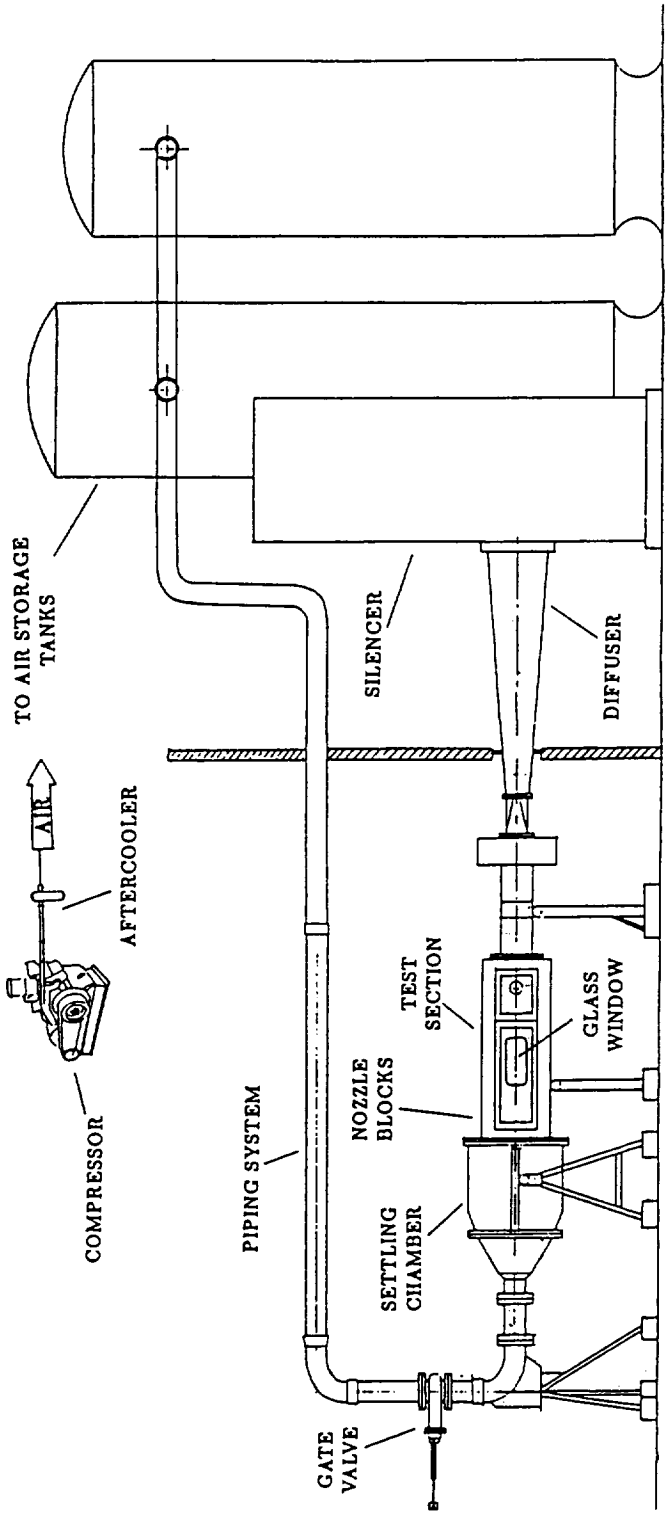

Figure 4 : Schematic drawing of the WSU 9 × 9-inch Supersonic wind tunnel.

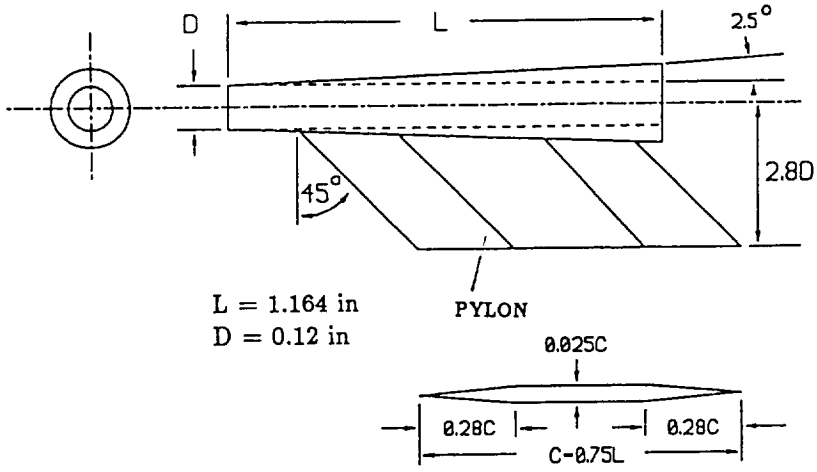

Figure 5 : Geometric details of nacelle/pylon.

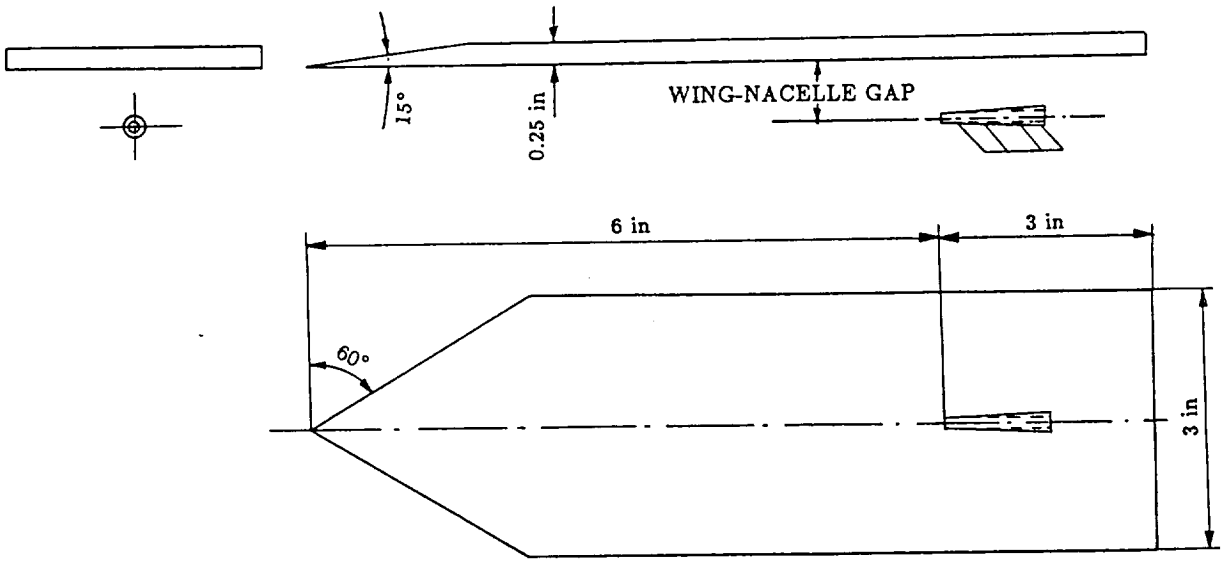

Figure 6 : Geometric details of simulated wing.

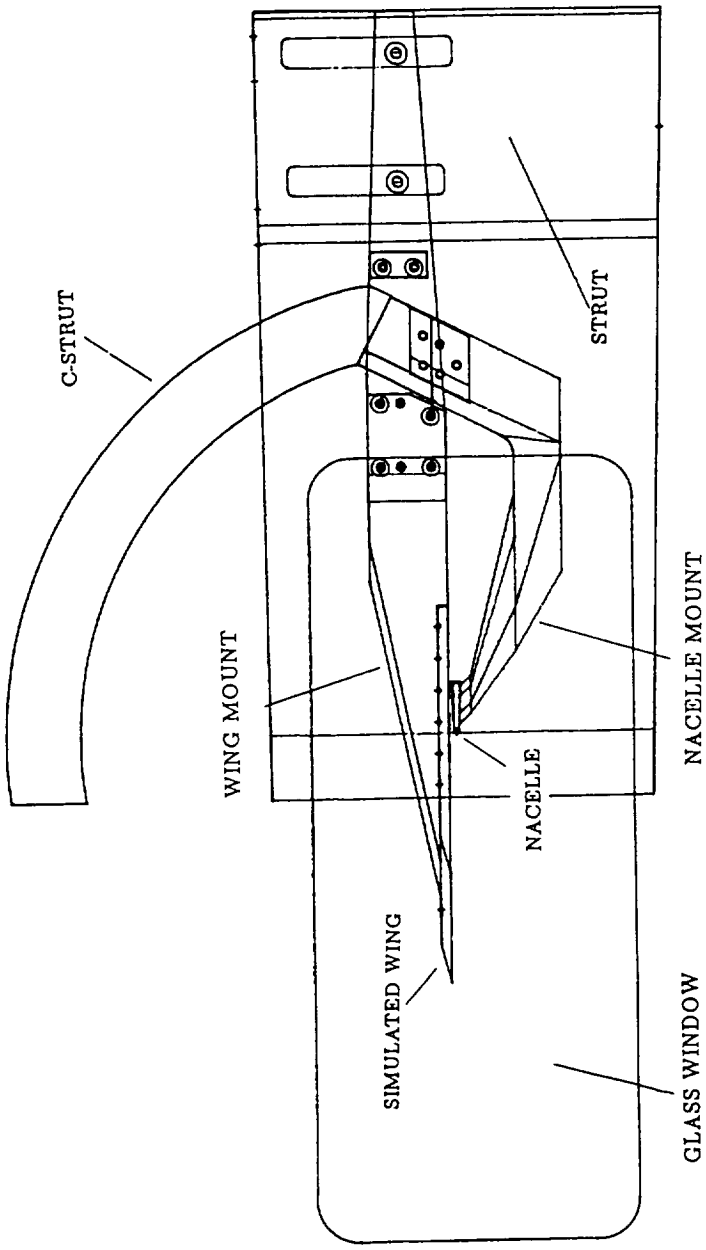

Figure 7 : Side view of nacelle in proximity to simulated wing and the model support system.

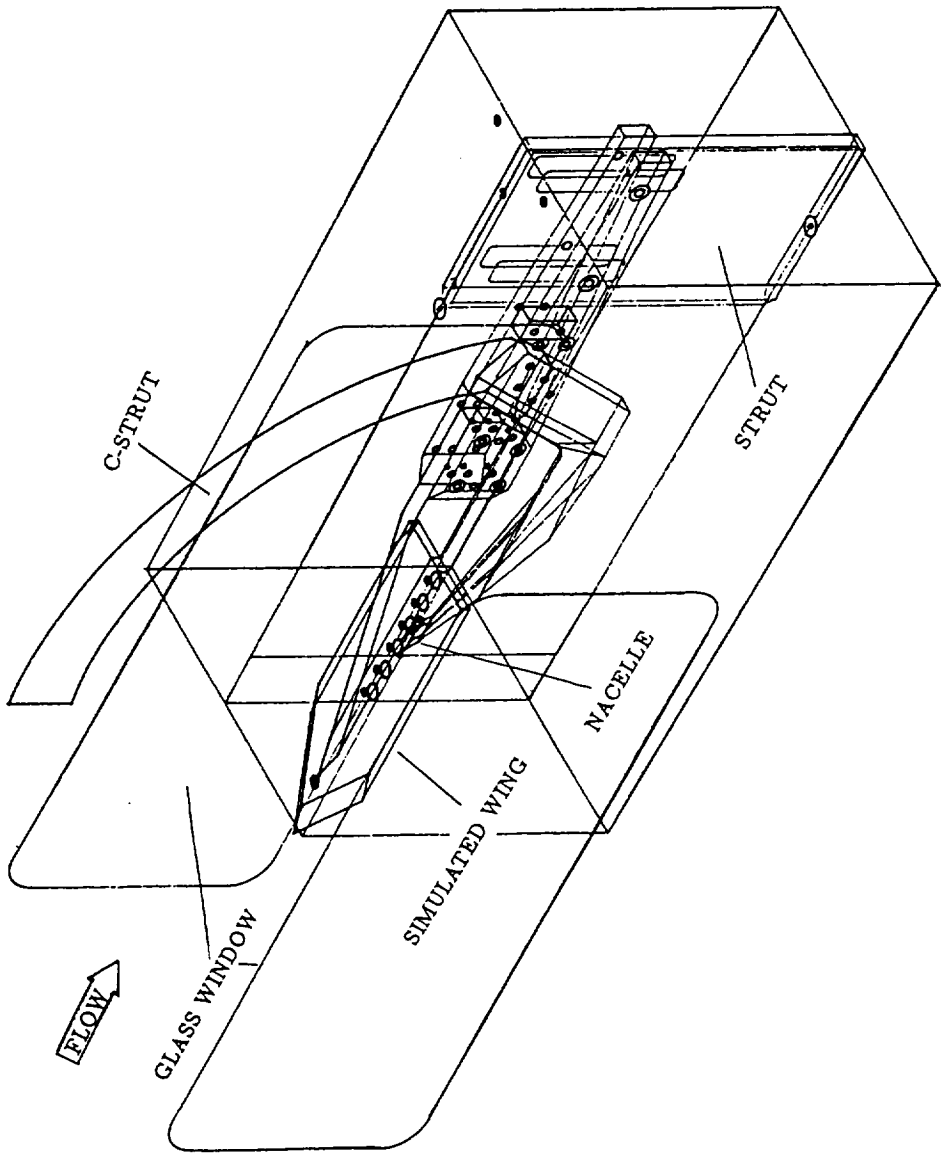

Figure 8 : Axi-symmetric view of nacelle and wing with sting mount, and C-strut assembly in the tunnel test section.

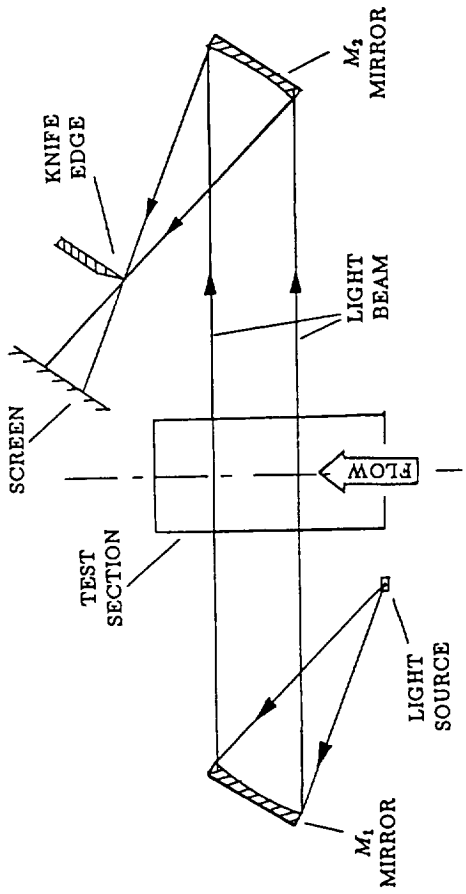

Figure 9 : Schlieren flow visualization set up with "Z" arrangement.

Figure 10 : Shock and expansion wave flow patterns over the nacelle at $Re_L = 1.45 \times 10^6$ and $\alpha = -2°$

Figure 11 : Shock and expansion wave flow patterns over the nacelle at $Re_L = 1.45 \times 10^6$ and $\alpha = 0°$

Figure 12 : Shock and expansion wave flow patterns over the nacelle at $Re_L = 1.45 \times 10^6$ and $\alpha = +2°$

Figure 13 : Shock and expansion wave flow patterns over the nacelle at $Re_L = 1.45 \times 10^6$ and $\alpha = +4°$

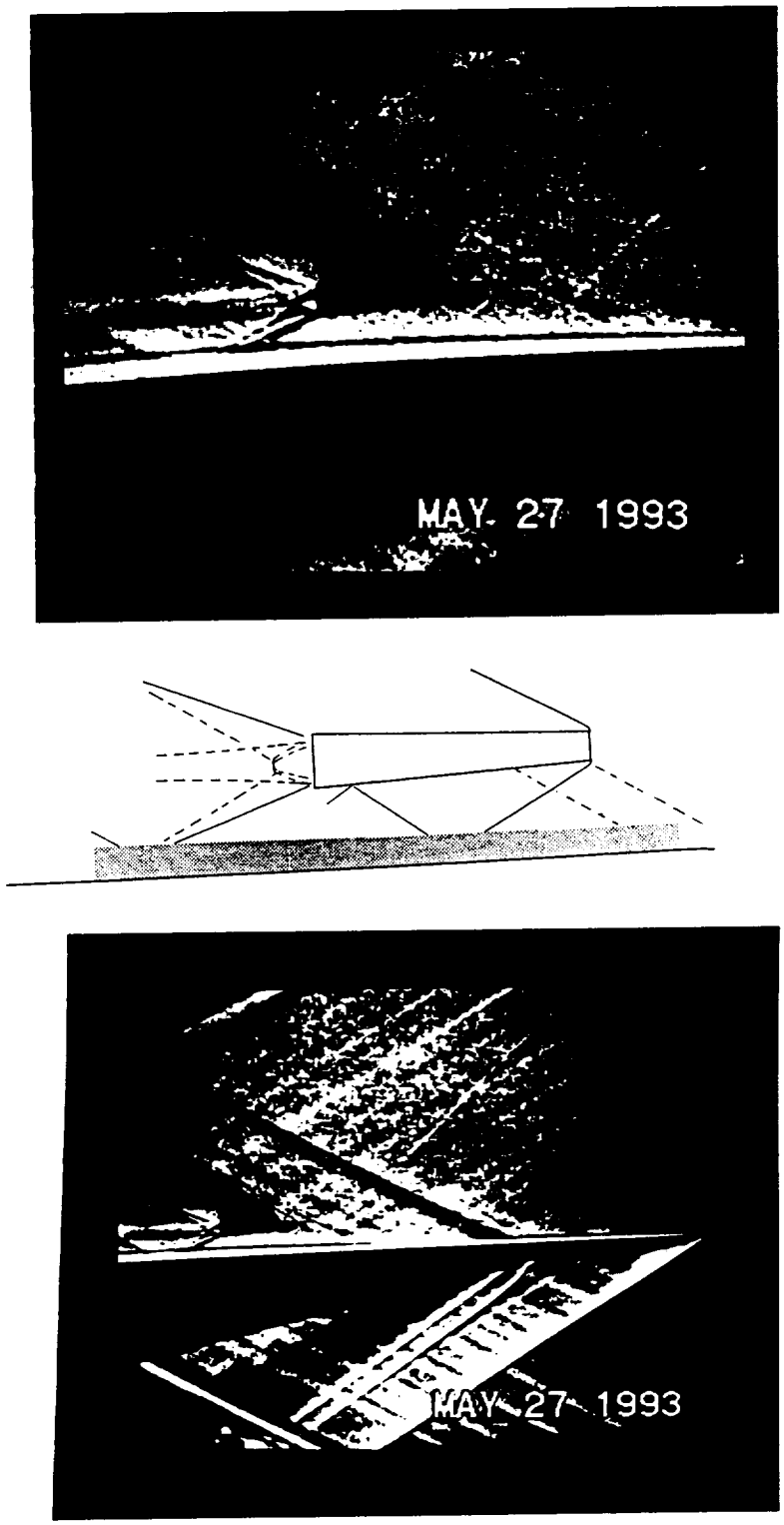

Figure 14 : Shock-boundary layer interaction between the nacelle and the wing for Y/D = 3 test case at $Re_L = 1.45 \times 10^6$ and $\alpha = -2°$.

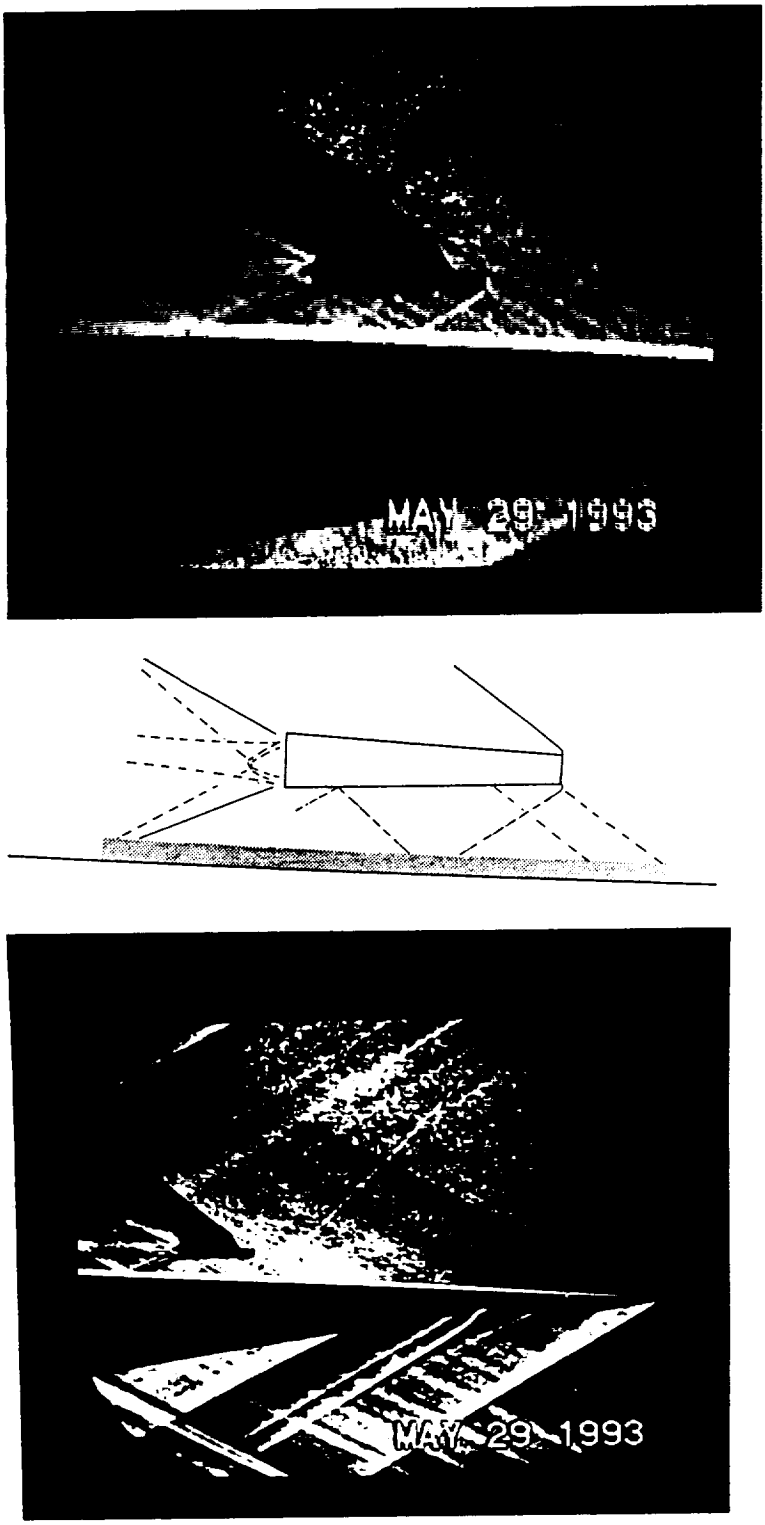

Figure 15 : Shock-boundary layer interaction between the nacelle and the wing for Y/D = 3 test case at $Re_L = 1.45 \times 10^6$ and $\alpha = +4°$.

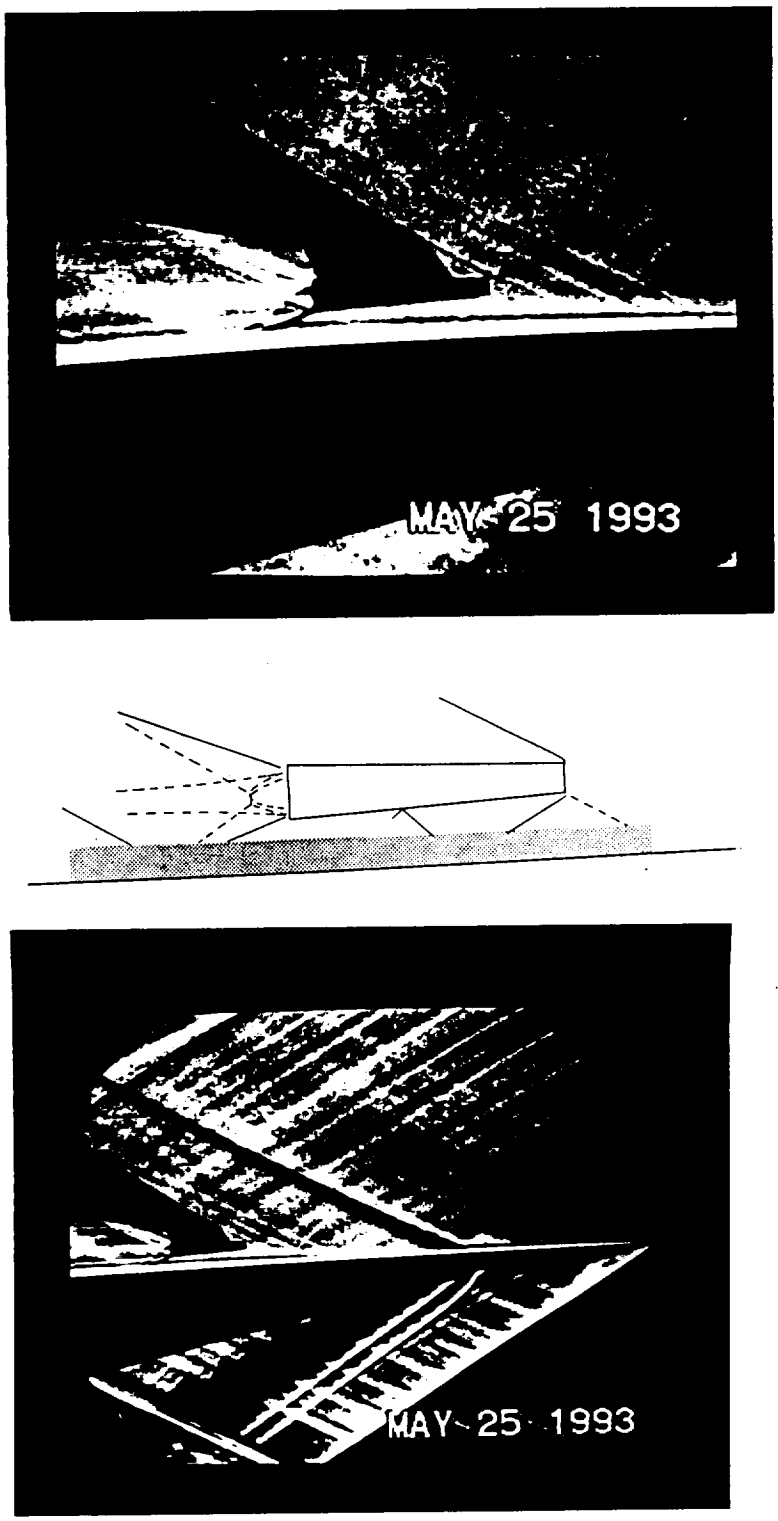

Figure 16 : Shock-boundary layer interaction between the nacelle and the wing for Y/D = 2 test case at $Re_L = 1.45 \times 10^6$ and $\alpha = -2°$.

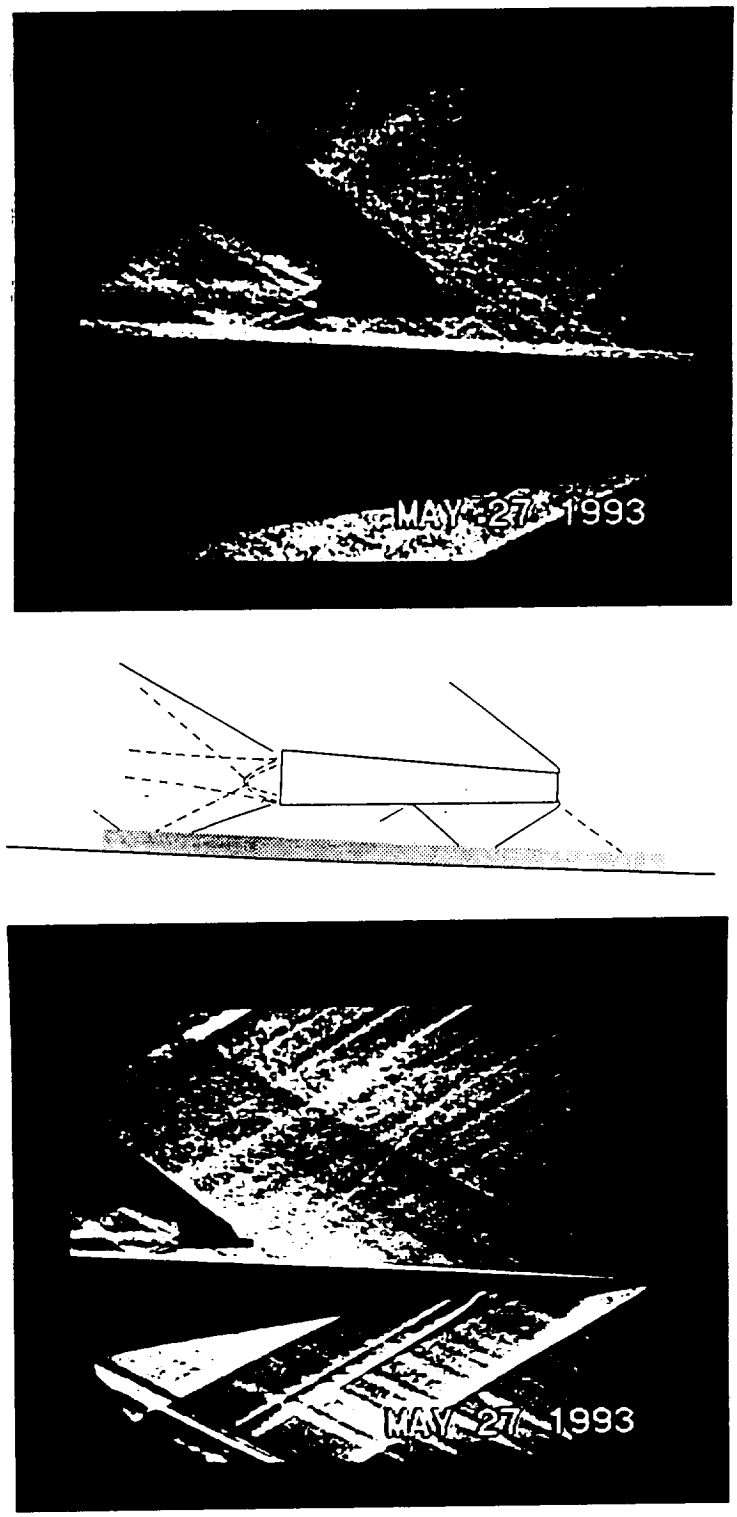

Figure 17 : Shock-boundary layer interaction between the nacelle and the wing for Y/D = 2 test case at $Re_L = 1.45 \times 10^6$ and $\alpha = +4°$.

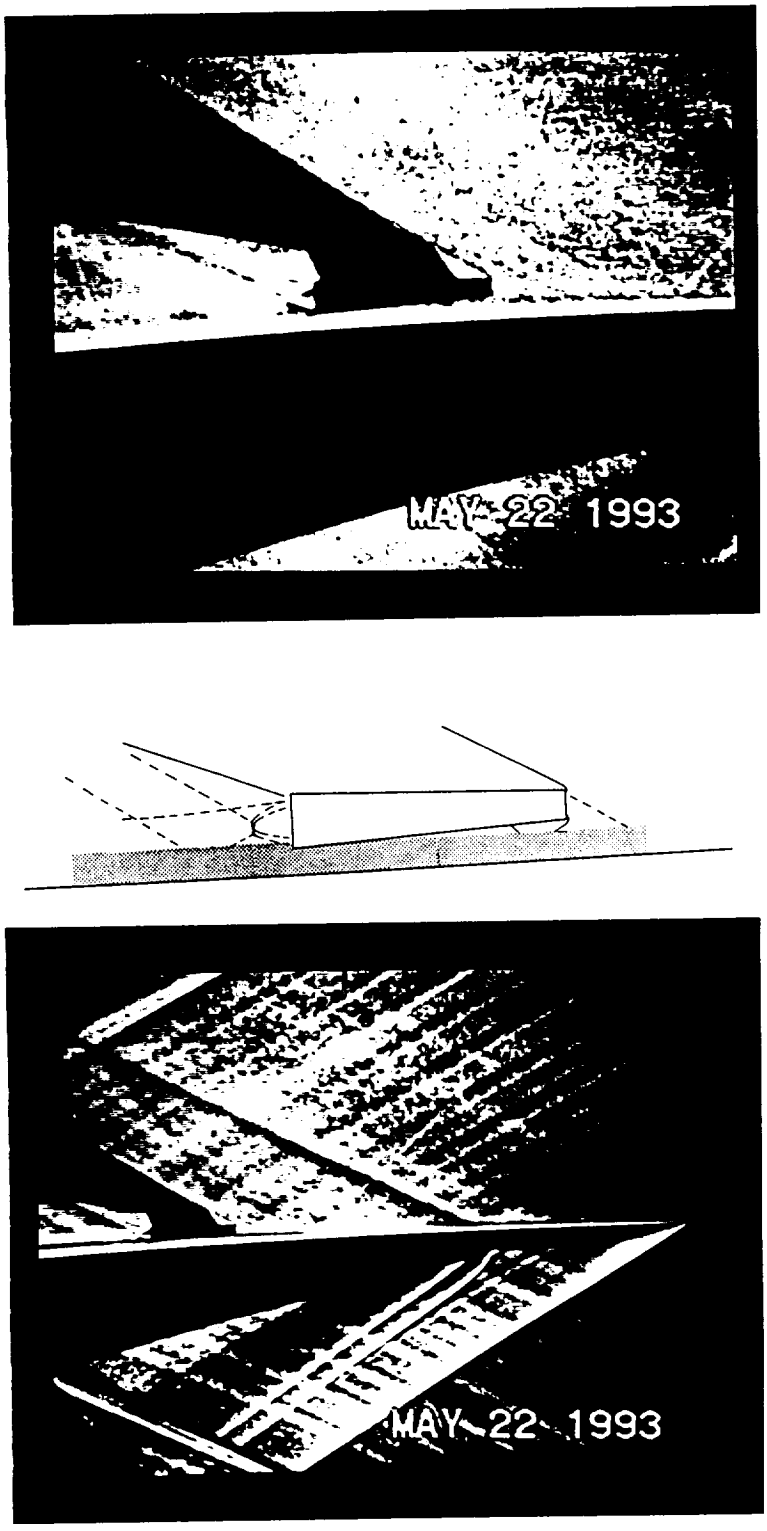

Figure 18 : Shock-boundary layer interaction between the nacelle and the wing for Y/D = 1 test case at $Re_L = 1.45 \times 10^6$ and $\alpha = -2°$.

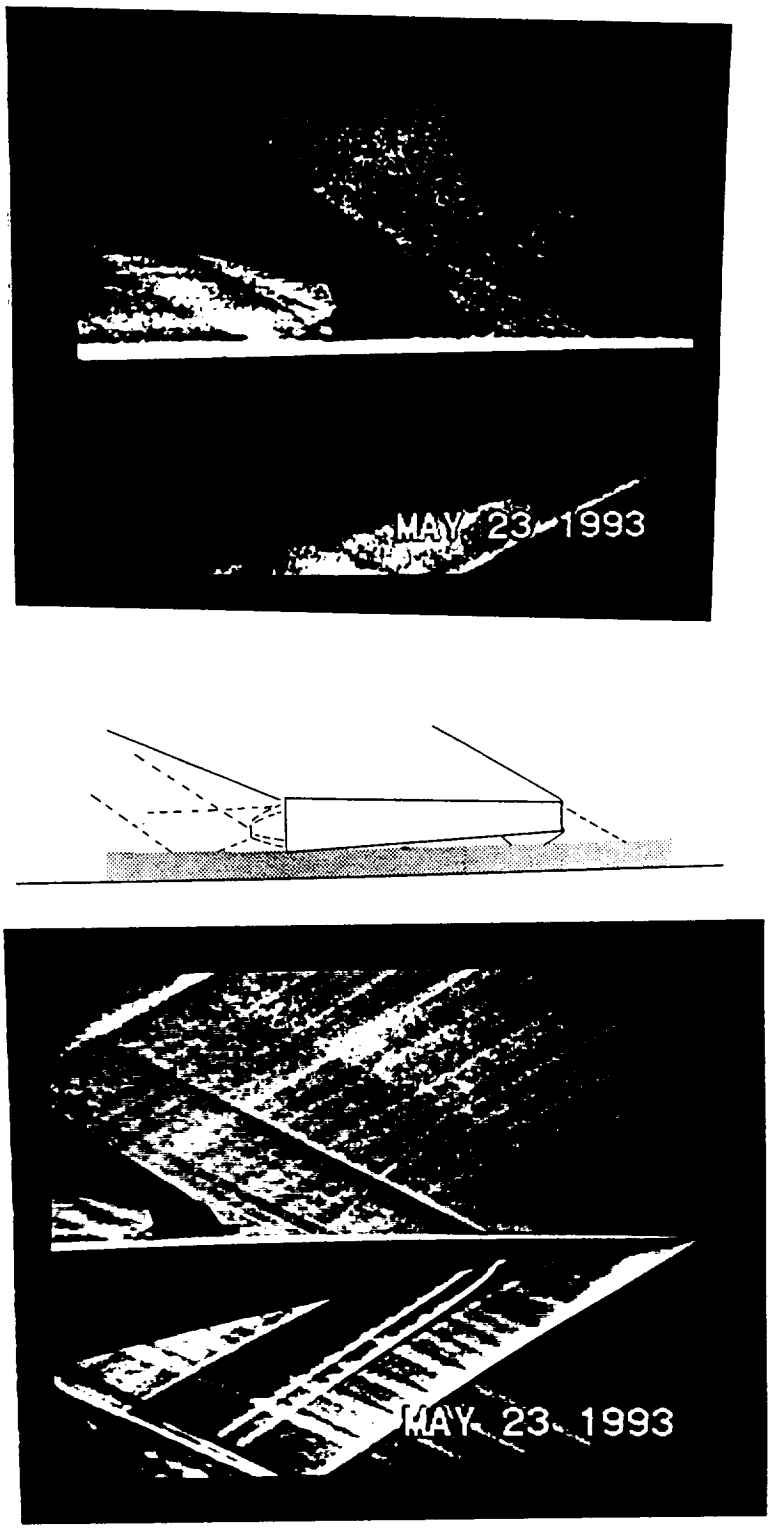

Figure 19 : Shock-boundary layer interaction between the nacelle and the wing for Y/D = 1 test case at $Re_L = 1.45 \times 10^6$ and $\alpha = 0°$.

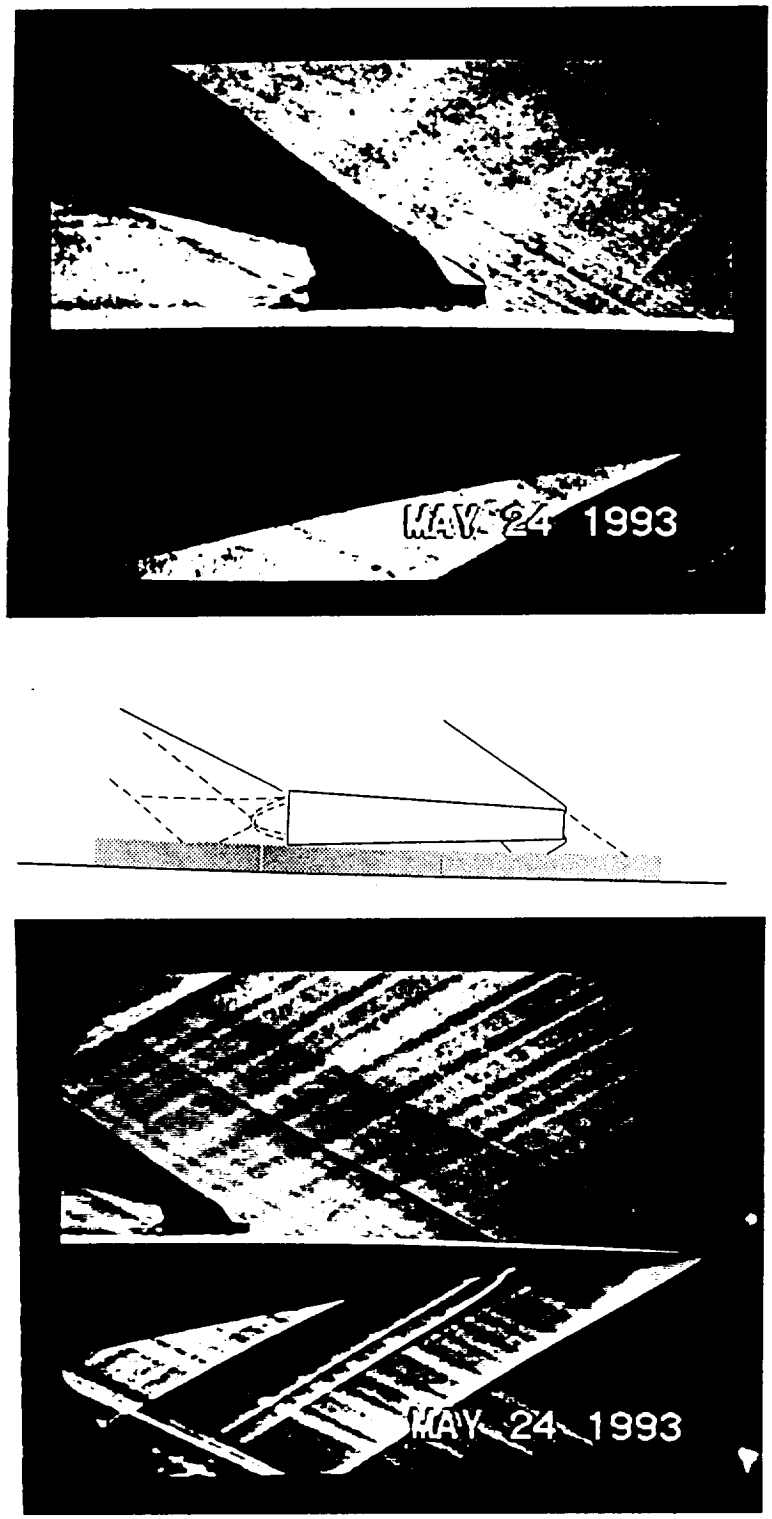

Figure 20 : Shock-boundary layer interaction between the nacelle and the wing for Y/D = 1 test case at $Re_L = 1.45 \times 10^6$ and $\alpha = +2°$.

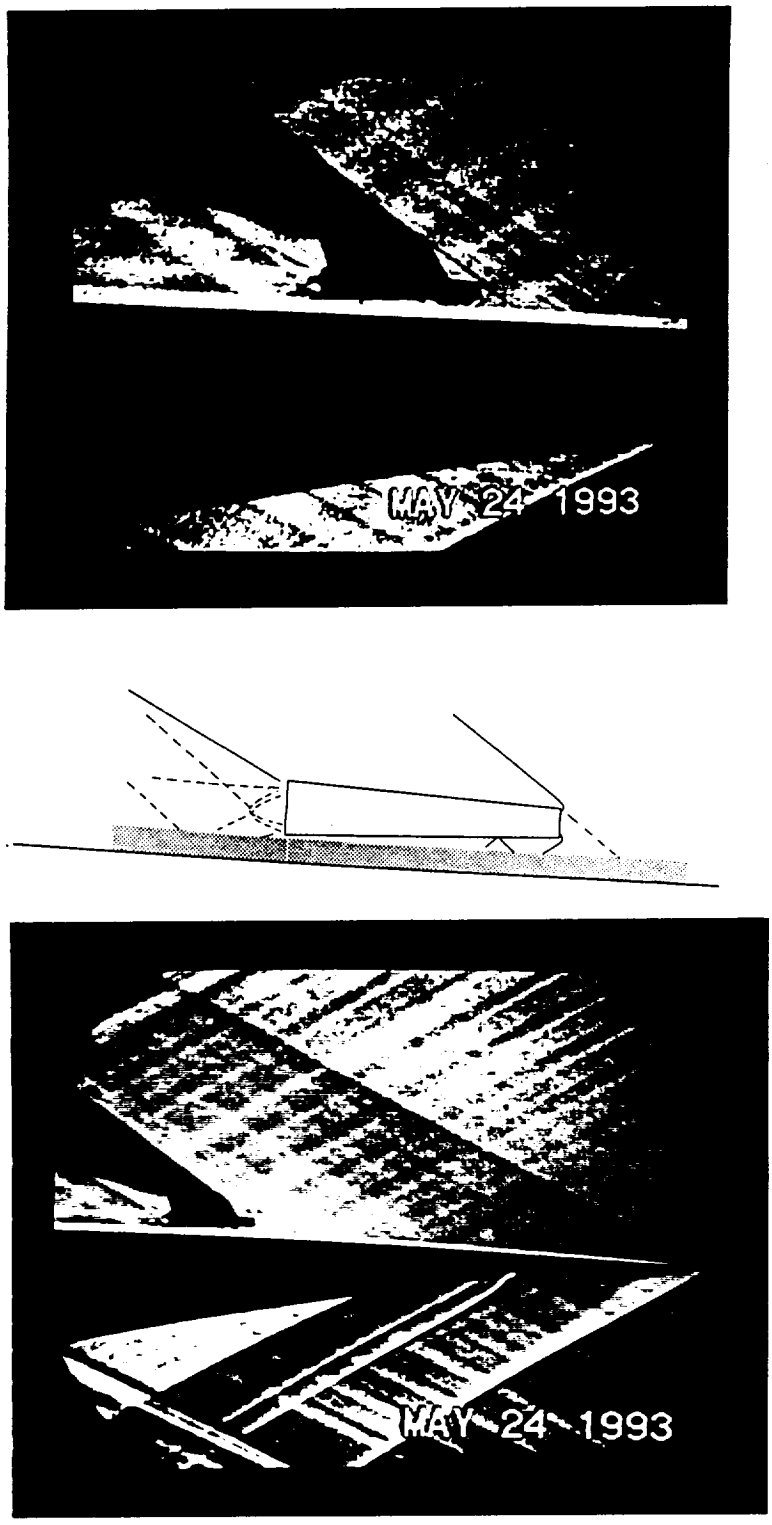

Figure 21 : Shock-boundary layer interaction between the nacelle and the wing for Y/D = 1 test case at $Re_L = 1.45 \times 10^6$ and $\alpha = +4°$.

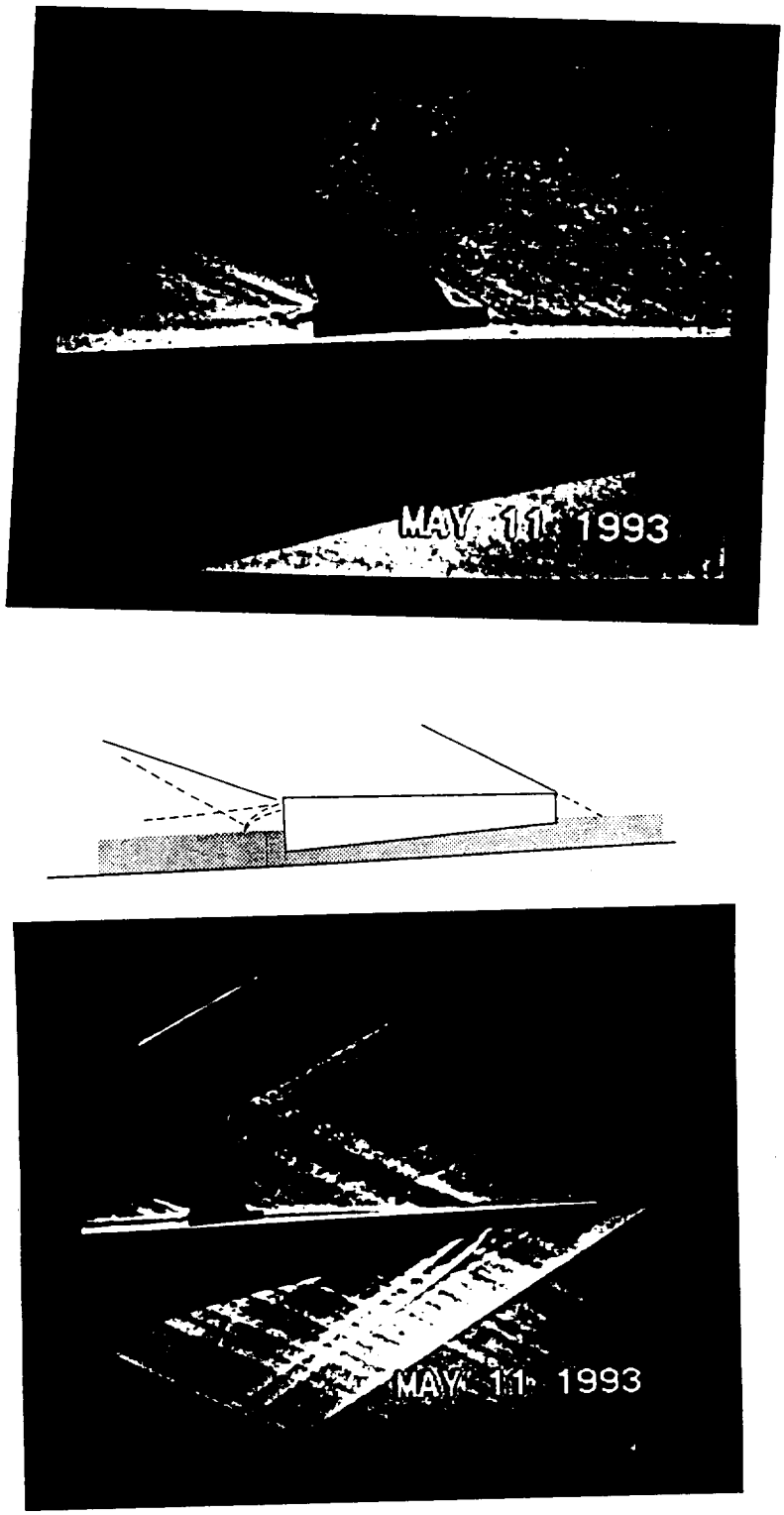

Figure 22 : Shock-boundary layer interaction between the nacelle and the wing for Y/D = 0.5 test case at $Re_L = 1.45 \times 10^6$ and $\alpha = -2°$.

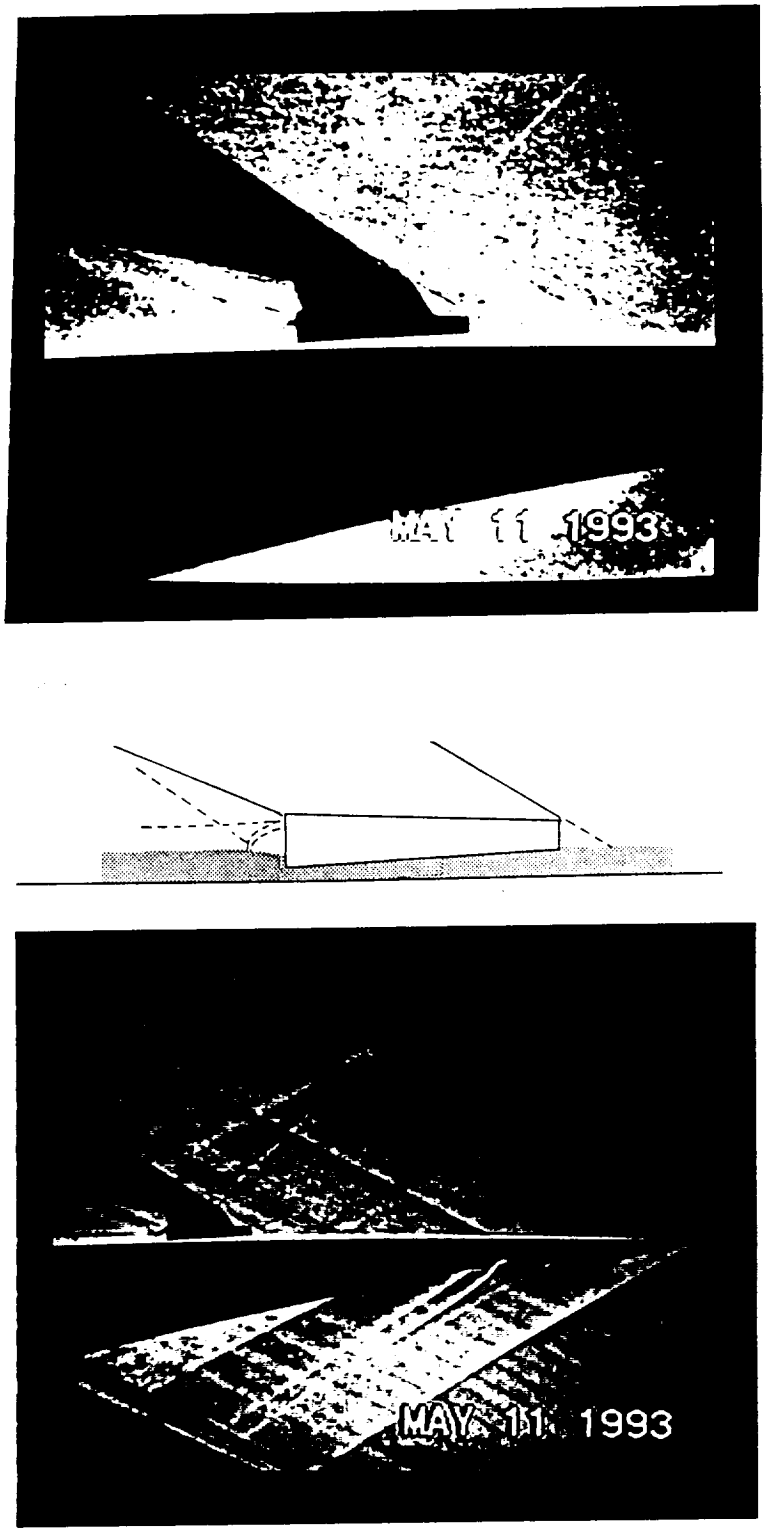

Figure 23 : Shock-boundary layer interaction between the nacelle and the wing for Y/D = 0.5 test case at $Re_L = 1.45 \times 10^6$ and $\alpha = 0°$.

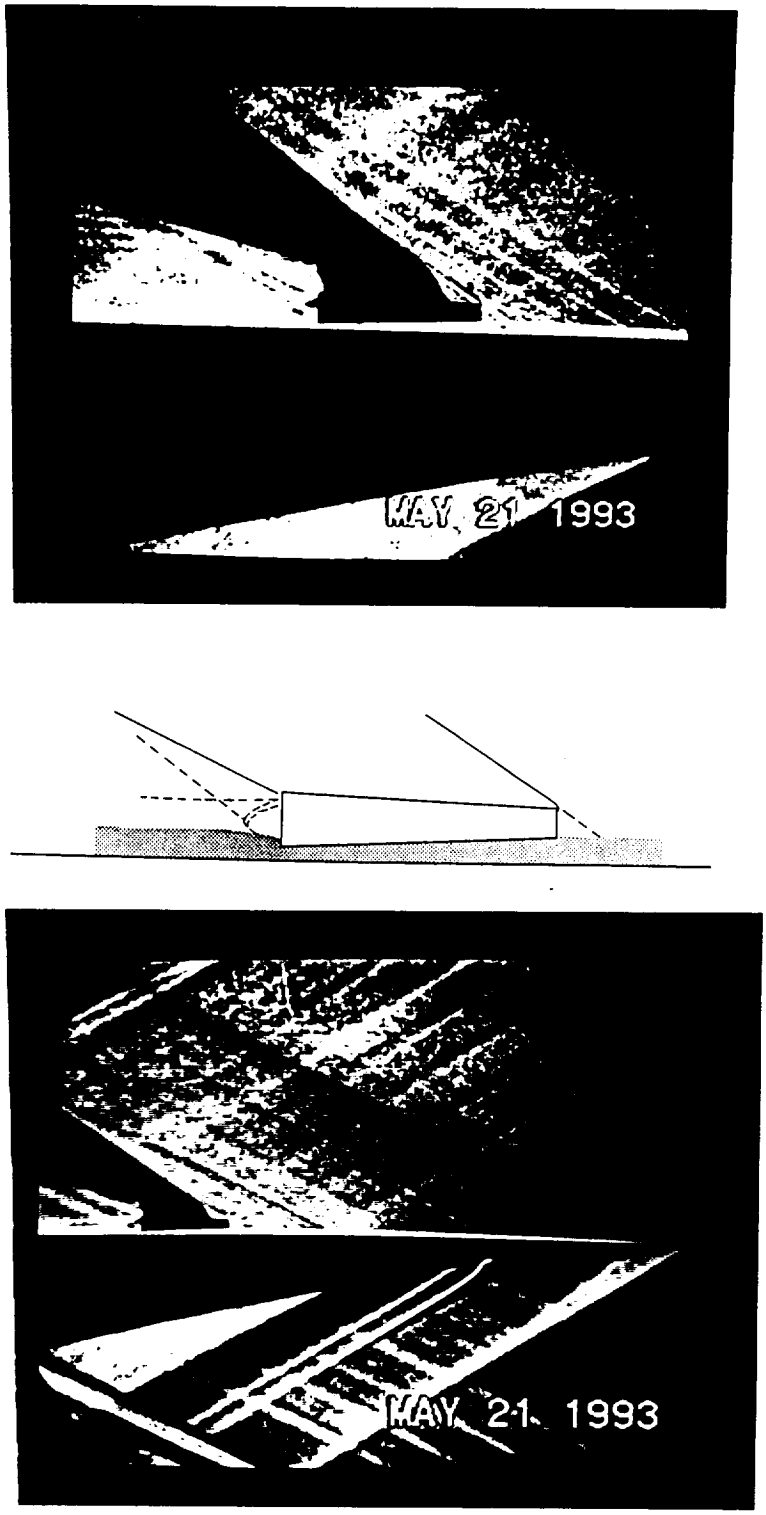

Figure 24 : Shock-boundary layer interaction between the nacelle and the wing for Y/D = 0.5 test case at $Re_L = 1.45 \times 10^6$ and $\alpha = +2°$.

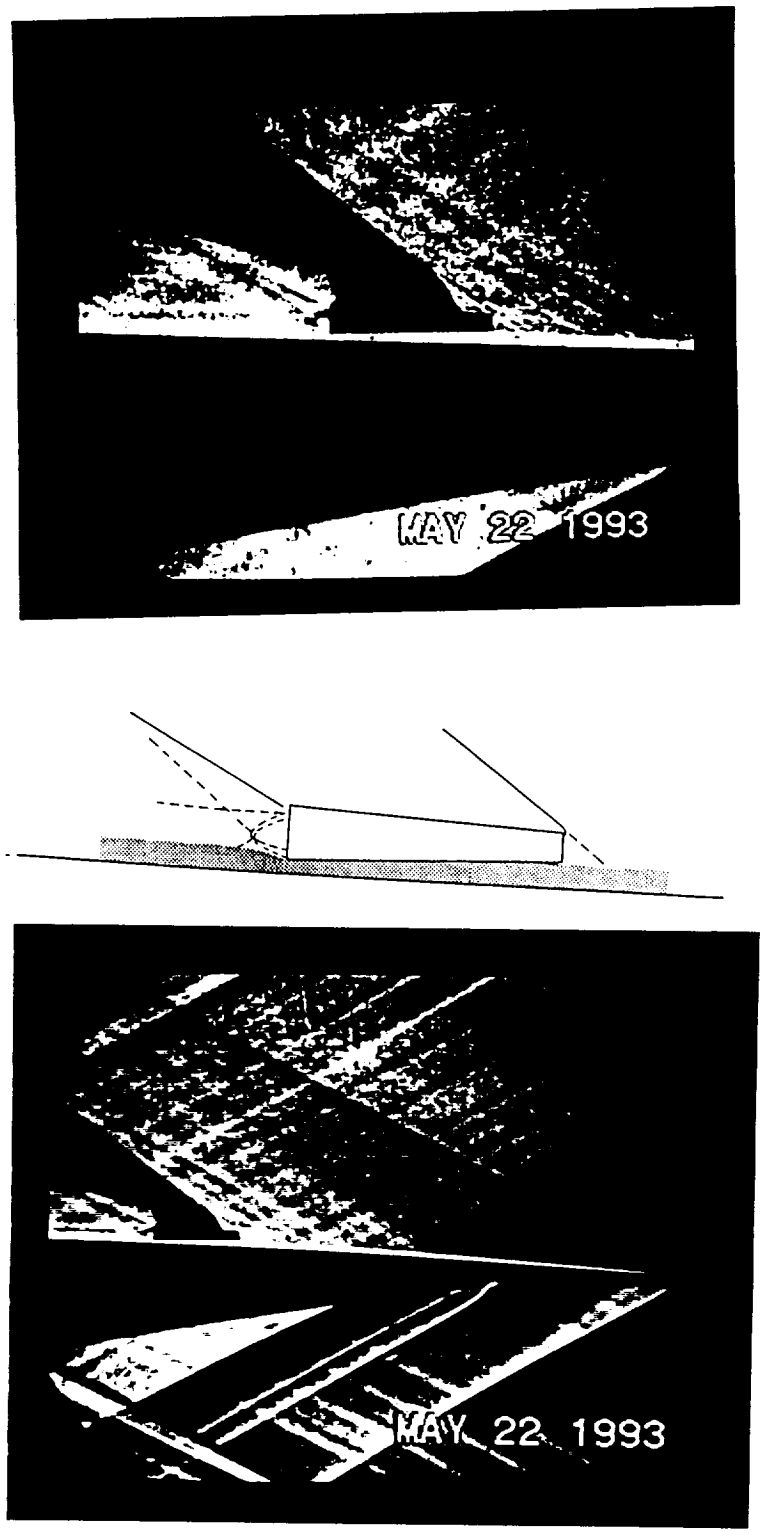

Figure 25 : Shock-boundary layer interaction between the nacelle and the wing for Y/D = 0.5 test case at $Re_L = 1.45 \times 10^6$ and $\alpha = +4°$.